NANO LETTERS
Letter
Cite This: Nano Lett. XXXX, XXX, XXX-XXX
pubs.acs.org/NanoLett

Role of Crystal Symmetry in the Reversibility of Stacking-Sequence Changes in Layered Intercalation Electrodes

Maxwell D. Radin,[†] Judith Alvarado,[‡,§] Y. Shirley Meng,[‡] and Anton Van der Ven*[,†]

[†]Materials Department, University of California Santa Barbara, Santa Barbara, California 93106-5050, United States
[‡]Department of NanoEngineering and [§]Materials Science and Engineering Program, University of California San Diego, La Jolla, California 92093, United States

Supporting Information

ABSTRACT: The performance of many technologies, such as Li- and Na-ion batteries as well as some two-dimensional (2D) electronics, is dependent upon the reversibility of stacking-sequence-change phase transformations. However, the mechanisms by which such transformations lead to degradation are not well understood. This study explores lattice-invariant shear as a source of irreversibility in stacking-sequence changes, and through an analysis of crystal symmetry shows that common electrode materials (graphitic carbon, layered oxides, and layered sulfides) are generally susceptible to lattice-invariant shear. The resulting irreversible changes to microstructure upon cycling ("electrochemical creep") could contribute to the degradation of the electrode and capacity fade.

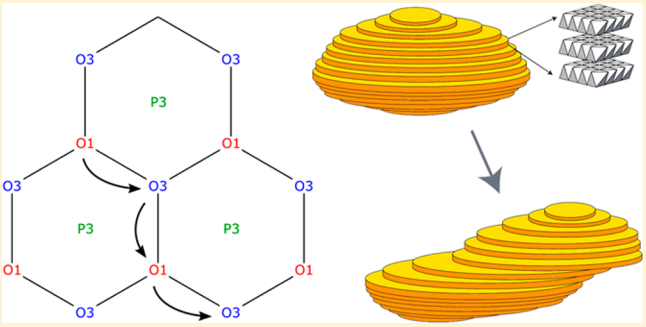

KEYWORDS: *Li-ion batteries, Na-ion batteries, layered materials, two-dimensional materials, fracture*

Layered materials play an important role in many fields because of their unique chemical, mechanical, and electronic properties. The exploitation of these properties by humans dates back at least 20,000 years to the invention of pottery, which leverages the dramatic changes in the mechanical properties of clay minerals as water is deintercalated.[1] State-of-the-art Li-[2−4] and Na-ion[5,6] batteries utilize the capability of layered materials to reversibly intercalate ions, while two-dimensional (2D) electronics[7] (e.g., graphene and MoS_2) and dry lubricants[8] utilize their electronic and mechanical properties. Novel applications of layered materials are now also being explored in the life sciences, where double layered hydroxides can serve as vessels for delivering drugs and biomolecules.[9]

Many of these applications involve a special type of phase transformation unique to layered materials: stacking-sequence-change phase transformations. In these transformations, each layer is topotactically preserved, but the relative alignment of the layers changes. Stacking-sequence changes occurring during the (de)lithiation of the classical Li-ion battery materials Li_xCoO_2[4,10,11] and lithium-intercalated graphite[12−15] are canonical examples, although stacking-sequence changes appear to be even more prevalent in Na-ion battery materials due to the stability of Na ions in both octahedral and prismatic environments.[4−6,16,17] Nickel (oxy)hydroxide, $NiOOH_{1+x}$, the active cathode material in NiMH, Ni−Cd, and Ni−Zn batteries similarly exhibits a change in stacking sequence upon electrochemical cycling.[18,19] Some novel nanoelectronic devices (e.g., devices based on MoS_2[20−22]) seek to exploit reversible changes in chemical and optical properties associated with stacking-sequence changes.

The reversibility of stacking-sequence changes is a critical factor in the performance of these devices. In particular, stacking-sequence changes may contribute to mechanical damage that occurs during the electrochemical cycling of common Li- and Na-ion battery materials.[4,23] For example, the formation of microcracks and accumulation of dislocations[4,24−28] has been widely observed in layered oxide cathodes. In graphitic anodes, the cracking of the solid-electrolyte interphase (SEI) has also been widely observed.[29] Although previous theoretical studies have examined the role of elastic strain arising from concentration gradients and two-phase coexistence in battery materials,[29,30] little is known about the exact mechanisms by which plastic deformation and irreversible changes to the microstructure occur.

This work proposes lattice-invariant shear as a mechanism for stacking-sequence-change phase transformations to induce degradation and extends the formalism developed by Bhattacharya et al. to ascertain which layered battery materials are susceptible to lattice-invariant shear.[31] The main result of Bhattacharya et al. was that one can gain insight in to the reversibility of displacive phase transformations through considerations of crystal symmetry. Their work focused on phase transformations in alloys driven by temperature or stress,

Received: September 15, 2017
Revised: October 21, 2017
Published: October 30, 2017

DOI: 10.1021/acs.nanolett.7b03989
Nano Lett. XXXX, XXX, XXX−XXX

such as the FCC (austentite) ↔ BCC (martensite) transformation in steel[32] and the related transformations occurring in shape-memory alloys.[33,34] Here we analyze layered battery materials, wherein the driving force for transformation is electrochemical.

Our main finding is that most layered battery materials, including graphite and common layered oxides and sulfides, are susceptible to lattice-invariant shear because of their crystal symmetry. This could result in irreversible changes to microstructure during cycling, an effect which we will refer to as "electrochemical creep". These changes may include the accumulation of extended defects and the changes in the shape of active-material particles, potentially contributing to particle fracture and the cracking of the SEI.

Lattice-Invariant Shear in Graphitic Systems. We first introduce the general concept of lattice-invariant shear in layered materials using as a prototype the AA ↔ AB transformation characteristic of alkali graphite intercalation compounds,[15] including lithium-intercalated graphite,[12−15] which serves as the anode material in nearly all commercial Li-ion batteries.[2,35,36] In these phases, the layers consist of a honeycomb lattice of carbon atoms, as shown in Figure 1. (A

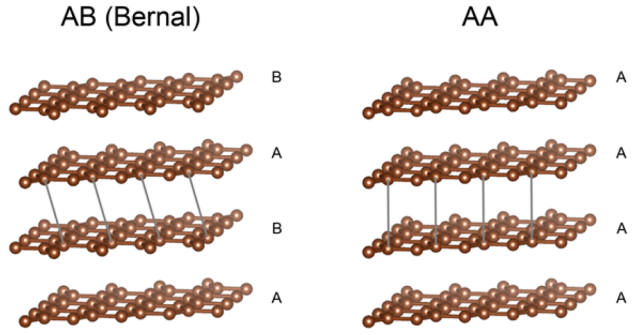

Figure 1. Stacking sequences in graphite.

honeycomb is not strictly speaking a lattice in the crystallographic sense but nevertheless is commonly referred to as a lattice.) We consider the relative alignment of two layers where the bottom layer is taken be in position A, and the top layer has three possible lateral positions: A, B, or C. In the absence of intercalation, graphite prefers an AB stacking (or the symmetrically equivalent AC) in which every other layer is staggered, as shown in the left panel of Figure 1. In a Li-ion battery with a graphitic anode, Li intercalates between the graphite layers upon charging to form LiC_6. This drives a stacking-sequence change from AB to AA, wherein the carbon layers are stacked directly on top of each other. Between the end members C and LiC_6, a number of staged compounds form wherein some layers form AB-type stacking and others form AA-type stacking.[12−15]

An AA → AB transformation between two layers followed by the reverse transformation, AB → AA, can lead to a lattice-invariant shear, that is, an overall shift in the relative alignment of layers. The first AA → AB transformation has three symmetrically equivalent glide pathways (as well as three symmetrically equivalent AA → AC pathways), shown in Figure 2. Similarly, the reverse transformation, AB → AA, has three symmetrically equivalent pathways. One of these three leads back to the original AA alignment of layers; however, the other two lead to AA stackings distinct from the initial state. Traversing one of these two pathways will result in an overall

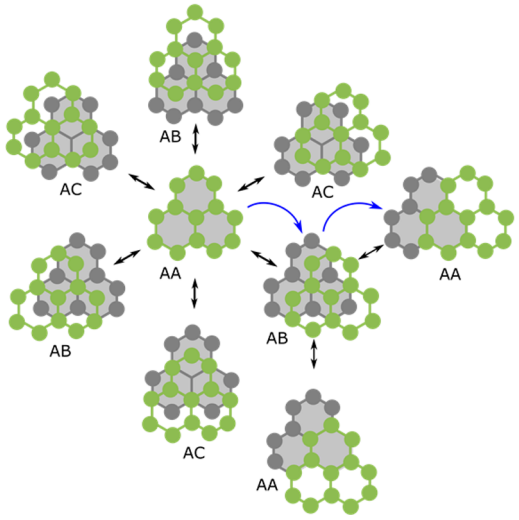

Figure 2. Stacking-sequence change pathways for graphite. Gray and green circles represent carbons atoms in the lower and upper layers. The blue arrows illustrate how the sequence of transformations AA → AB → AA can result in lattice-invariant strain.

shift in the relative alignment of layers relative to the starting configuration, as represented by the blue arrows in Figure 2. Thus, these AA → AB → AA pathways result in a lattice-invariant shear of the original AA phase.

This lattice-invariant shear can be visualized as a path along the graph shown in Figure 3. The spatial dimensions of this

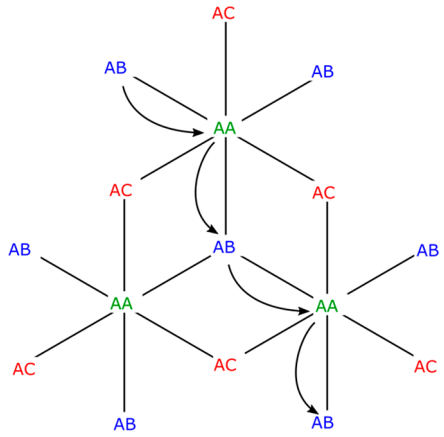

Figure 3. Stacking sequence change pathways in graphite. The arrows show one possible pathway for lattice-invariant shear.

figure correspond to the relative alignment of adjacent layers and the nodes represent AA, AB, and AC stackings. Lines connecting nodes represent pathways accessible during a charge or discharge cycle. Lattice-invariant shear manifests as the infinite connectivity of the graph formed by these pathways. (The graph shown in Figure 3 is sometimes referred to as a "dice lattice", although the nodes themselves form a triangular lattice.) In the language used to describe martensitic transformations, an infinite connectivity represents a "strong" phase transformation, while a bounded graph represents a "weak" one.

While the transformations between different stacking sequences can be thought of as a simple gliding of the slabs, the crystallography is complicated by the fact that stacking-sequence changes also involve other degrees of freedom. At a minimum, this includes an isotropic in-plane expansion or

DOI: 10.1021/acs.nanolett.7b03989
Nano Lett. XXXX, XXX, XXX−XXX

contraction of the layers as well as a change in their separation. In other cases, there may also be an anisotropic distortion of the slabs (e.g., elongation along x and contraction along y), as well as a relative displacement of sites within each slab. In the Supporting Information, we derive a formalism that allows such transformations to be mapped onto a two-dimensional space describing stacking, such as that shown in Figure 3.

Lattice-Invariant Shear in Layered Oxides and Sulfides. Applying this formalism to the stacking-sequence changes that occur in the layered oxides and sulfides commonly used as Li-[2−4] and Na-ion[5,6] battery electrodes shows that these materials are also susceptible to lattice-invariant shear. The layered oxides/sulfides have formula A_xMX_2, where the alkali metal A intercalates in between MX_2 layers (M = transition metal and X = oxygen or sulfur). When used as a cathode, $x = 1$ corresponds to the fully discharged battery and $x = 0$ the fully charged one. Each MX_2 layer consists of three atomic planes (X−M−X) with each atomic plane occupying the A, B, or C sublattice of a triangular lattice. The M sites will be either octahedrally or prismatically coordinated, depending on whether or not the two X planes occupy the same triangular sublattice. We focus now on the octahedral case, as this is the coordination for the most common battery materials.

Assuming the transition metals reside in octahedral sites, six "primitive" layered structures can be generated by enumerating the possible stacking sequences of two adjacent MX_2 layers (Figure 4): O1, O3, P3, O2(a), O2(b), and P2. These

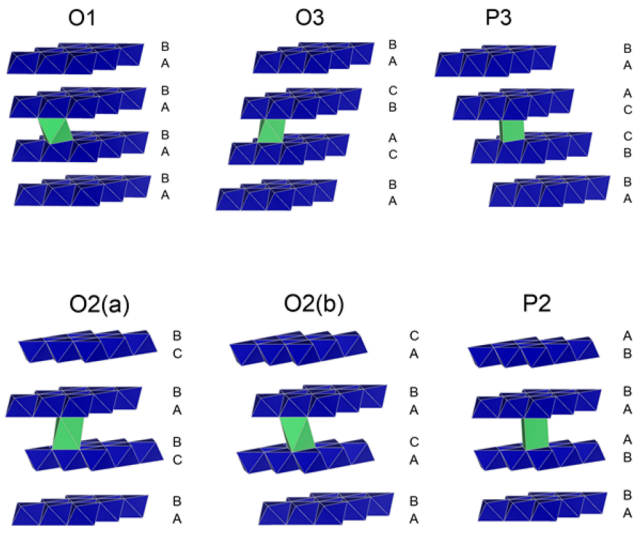

Figure 4. Crystal structures for common layered dichalcogenides. Vertices represent anion sites, while transition metals reside at the centers of blue polyhedral and intercalants at the centers of green polyhedral. The labels A, B, and C denote the positions of the anion sublattice.

structures are primitive in the sense that all other layered octahedral dichalcogenide structures (e.g., H1−3[37,38]) can be constructed by interleaving them. We follow the nomenclature of Delmas et al.,[39] wherein the letter refers to the coordination of intercalant sites (octahedral or prismatic) and the number indicates the number of layers in the repeat unit. Although O2(a) and O2(b) are equivalent by a 180° rotation along an axis in the plane of the layers and are both commonly referred to as O2, we distinguish between them because they are not equivalent by lateral translation; as a result, their intergrowth would lead to the formation of extended defects.[40]

Phase transformations within this family of layered oxides and sulfides represent stacking-sequence changes, and these stacking-sequence changes can lead to lattice-invariant shear. The most common stacking-sequence changes in these materials are associated with the gliding of MX_2 layers, which results in transformation among O1, O3, and P3, and also among O2(a), O2(b), and P2. Transformations between the O1−O3−P3 and O2−P2 systems are rare because these require stacking-sequence changes within individual MX_2 layers, which are usually kinetically unfavorable because of strong M−X bonds. (However, one prominent example of stacking-sequence changes within a layer is the P2 ↔ O1 transformation of layered MoS_2;[7,20−22] these phases are frequently referred to as 2H and 1T in the context of 2D electronics.)

The most common stacking-sequence change in layered Li-ion cathode materials is from O3 to O1 (and O1/O3 hybrids) upon deep deintercalation (i.e., extreme charging).[4] This is observed in the classical layered oxides Li_xCoO_2[10,11] and Li_xNiO_2,[41] as well as the $Li_xNi_yMn_zCo_{1-y-z}O_2$ (NMC) solid solutions used in state-of-the-art commercial Li-ion cells.[23] The lattice-invariant shear of the O1 ↔ O3 transformation can be visualized as a honeycomb graph, as shown in Figure 5a.

Layered Na-ion battery materials differ from their Li analogues in that they often favor prismatic coordination at intermediate compositions ($x \sim 0.5$).[4−6,16,17] As a result, the partial deintercalation of O3 Na_xMX_2 often results in transformation to P3, and complete deintercalation to O1. The resulting O3 ↔ P3 and P3 ↔ O1 transformations result in

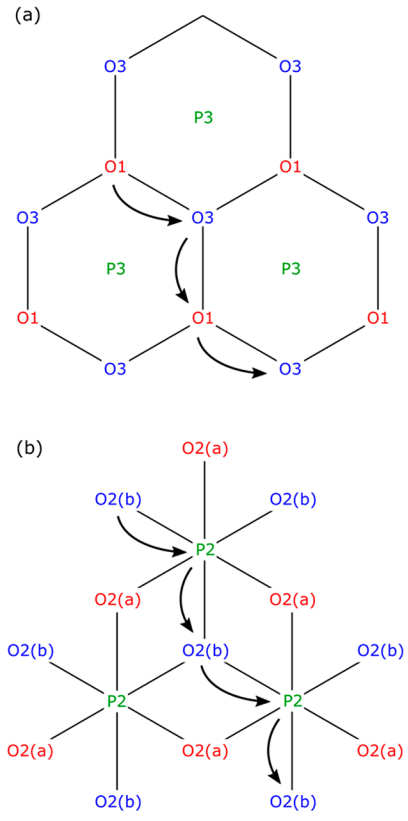

Figure 5. Stacking sequences in the (a) O1/O3/P3 system and (b) O2/P2 system. The arrows show one possible pathway for lattice-invariant shear for O3 ↔ O1 transformations and O2 ↔ P2 transformations.

DOI: 10.1021/acs.nanolett.7b03989
Nano Lett. XXXX, XXX, XXX−XXX

lattice-invariant shear represented by a honeycomb graph, like the O3 ↔ O1 transformation. The deintercalation of O2 Na_xMX_2 similarly can result in a transformation to P2.[5,6,42] This results in lattice-invariant shear along a dice lattice, as shown in Figure 5b.

To explore how electrochemical creep might contribute to the mechanical damage of layered battery materials upon cycling, we now explore how lattice-invariant shear might affect microstructure. One possible effect is changes to the particle shape. To illustrate this, we simulated the evolution in morphology of a crystallite over repeated O2 ↔ P2 transformations. Figure 6 shows the deformation of the particle

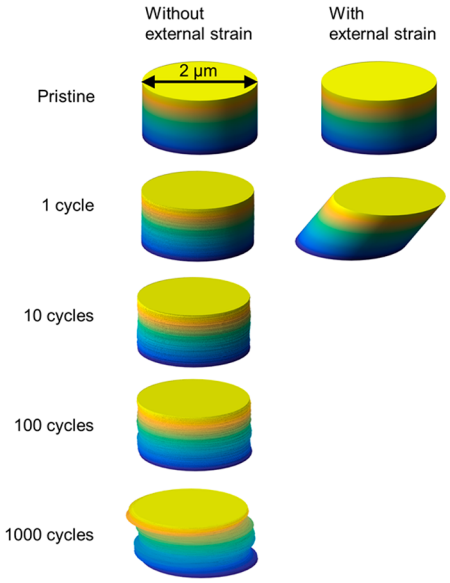

Figure 6. Simulated deformation of a layered oxide particle due to lattice-invariant strain arising from O2 ↔ P2 stacking-sequence changes during intercalation. The particles are 2 μm in diameter and 1 μm thick (2727 layers) and are assumed to have an a lattice parameter of 2.9 Å.

in two limiting cases. The left column represents deformation in the absence of external forces in which case each layer would be equally likely to slide in each of the symmetrically equivalent directions. Lattice-invariant shear results in a gradual roughening of the particle's surface over (de)intercalation cycles. The expected displacement of two layers (in the root-mean-square sense) is $a\sqrt{N_{\text{layers}}N_{\text{cycles}}}$, where a is the in-plane lattice parameter, N_{layers} is the number of layers between the two layers in question, and N_{cycles} is the number of cycles (see Supporting Information for details). In contrast, when a large resolved shear stress acts on the particle (for example, due to the contact forces with other particles), layers may preferentially slide in the direction that relieves the stress. The right column of Figure 6 illustrates a simulation of the limiting case where every layer slides in the same direction. After only a single cycle, the particle is dramatically distorted.

Another possible consequence of stacking-sequence changes is the accumulation of extended defects (i.e., dislocations) generated when different regions in a particle undergo lattice-invariant shear in different directions. For example, suppose during the deintercalation of AA graphite, one side of a particle nucleates AB while the other nucleates the symmetrically equivalent stacking AC in the same layer (Figure 7). The AA/

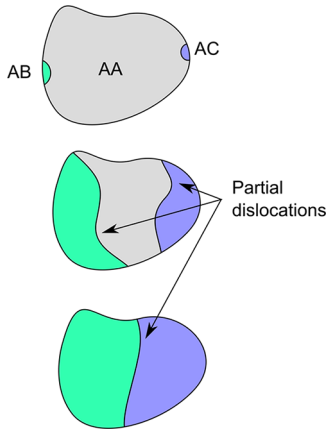

Figure 7. Example of a dislocation generated by lattice-invariant shear.

AB and AA/AC boundaries represent partial dislocations,[43] and as AA is converted to AB and AC, these partial dislocations glide across the particle. (Other nucleation and growth geometries, such as core−shell growth, are also possible, but do not change the underlying mechanism for dislocation accumulation.) After transformation is complete, the partial dislocations combine to form a dislocation separating the AB and AC regions. Similarly, the nucleation of two different AB variants or two different AC variants could also lead to dislocation accumulation.

Motivated by the role of slip in classical fatigue mechanisms,[44,45] we speculate that electrochemical creep could furthermore promote fracture during electrochemical cycling. For example, stresses associated with lattice expansion/contraction[4,46,47] could be concentrated by the surface roughness arising from electrochemical creep (cf. Figure 6), resulting in crack initiation. The accumulation of dislocations (cf. Figure 7) could similarly contribute to in a build-up in stress.

Although the direct observation of electrochemical creep and its impact on microstructure would be challenging, some signatures of these phenomena can be seen in prior experiments. For example, the scanning electron microscope (SEM) images shown in Figure 8 (obtained from the experiments described in ref 48) show the effect of electrochemical cycling on P2 $Na_{2/3}Ni_{1/3}Mn_{2/3}O_2$, a material that undergoes a P2 ↔ O2 stacking-sequence change at 4.2 V.[42] While the particles are intact in the pristine material (Figure 8a) and the uncycled composite electrode (Figure 8b), many steps and microcracks are present after 100 cycles to 4.5 V at a C/20 rate (Figure 8c). We hypothesize that these steps are the result of electrochemical creep (similar to the simulated particle morphologies in Figure 6), and that such steps may have contributed to the initiation of the cracks visible on the top part of the particle.) These microstructural changes may contribute to the loss in capacity and increase in polarization with cycling, as can be seen in the voltage curves shown in Figure 9.

The changes in microstructure arising from electrochemical creep could negatively impact battery performance in several ways. For example, microcracks can expose fresh active material to the electrolyte, contributing to the growth of any surface passivation layers.[4,48] Microcracks can also result in poor electronic connectivity between the active material and current collector.[27] Even if the active material does not fracture, changes in particle shape could crack the SEI or other

DOI: 10.1021/acs.nanolett.7b03989
Nano Lett. XXXX, XXX, XXX−XXX

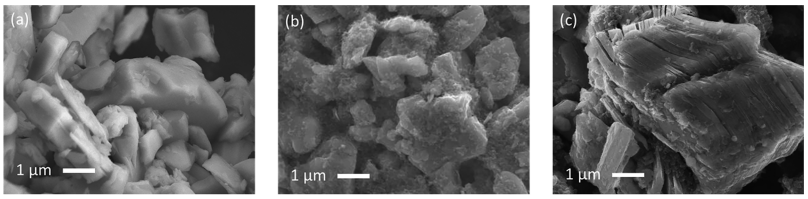

Figure 8. SEM images from the experiments of ref 48 showing (a) pristine layered $Na_{2/3}Ni_{1/3}Mn_{2/3}O_2$; (b) a $Na_{2/3}Ni_{1/3}Mn_{2/3}O_2$ composite electrode before cycling; (c) a $Na_{2/3}Ni_{1/3}Mn_{2/3}O_2$ composite electrode after 100 cycles.

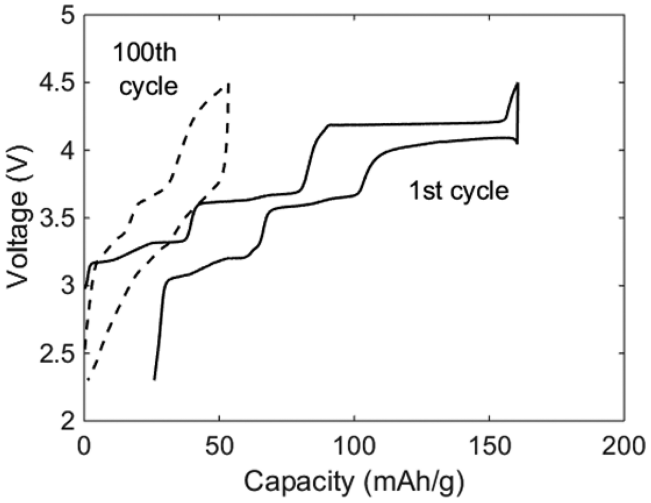

Figure 9. Comparison of the voltage profiles of cycles 1 and 100 for a P2−$Na_{2/3}Ni_{1/3}Mn_{2/3}O_2$ composite electrode cycled galvanostatically at a C/20 rate in the experiments of ref 48.

passivation layer and expose fresh active material to the electrolyte.

Creep can also arise from stacking-sequence changes induced by ion exchange. Yabuuchi et al. reported that Na^+/Li^+ ion exchange in OP4 $Li_xNa_yCoO_2$ resulted in the formation of ridges on particle surfaces.[49] We hypothesize that these ridges (shown in Figure 5 of ref 49) are the product of creep associated with the OP4 → O4 stacking-sequence change that occurred during these ion exchange experiments.

As discussed in the Supporting Information, the presence of lattice-invariant shear in common stacking-sequence-change transformations is a consequence of the symmetry of these phases. This suggests that modifications to the crystal structure that reduce the symmetry could potentially prevent, or at least impede, electrochemical creep by biasing the system to prefer some glides over others. Common symmetry-breaking modifications to layered structures include the presence of a collinear Jahn−Teller distortion (common in the layered Mn, Ni, and Cu oxides[50]), the ordering of intercalant cations (especially row orderings near $x = 0.5$[11,51,52]) and the ordering of cations in the transition-metal layer of oxides.

As an example, we consider how a $\sqrt{3} \times \sqrt{3}$ ordering within the transition-metal layer affects transformations between O1 and O3. This type of ordering is seen in many layered oxides, such as the "Li-excess" layered oxides derived from Li_2MnO_3.[53−57] Figure 10 shows the possible O1- and O3-type stacking sequences in such a material. All of the O3-type stackings (Figure 10a) are symmetrically equivalent. (These are denoted as O3′ because the transition-metal ordering lowers the symmetry from rhombohedral to monoclinic.) In contrast, there are two distinct O1 stackings: one that places the $\sqrt{3} \times$

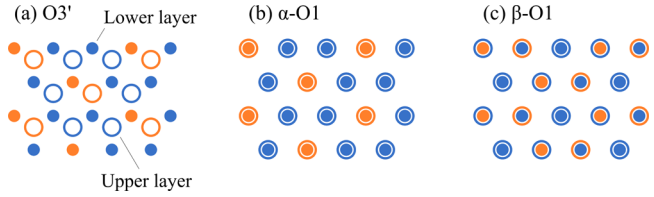

Figure 10. Arrangement of cations in the (a) O3′, (b) α-O1, and (c) β-O1 stacking sequences of a layered oxide with the Li_2MnO_3-type ordering within the transition-metal layers. The filled circles represent transition-metal sites in the upper layer, and the empty circles represent transition-metal sites in the lower layer. The color indicates which species resides at that site: blue corresponds to Mn and orange Li.

$\sqrt{3}$ ordering of one layer directly below the next (Figure 10b), and one in which the orderings are offset (Figure 10c). We shall refer to these to structures as α-O1 and β-O1. Figure 11 shows

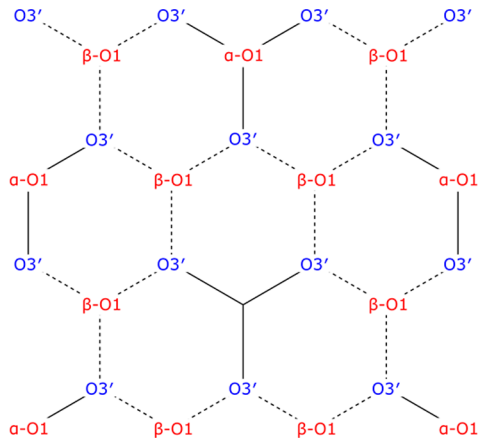

Figure 11. O1- and O3-type stacking sequences in a layered material with the Li_2MnO_3 ordering in the transition-metal layer.

the graph representing stacking-sequence changes in this system. If transformations from O3′ to α-O1 are strongly favored over transformations from O3′ to β-O1, then lattice-invariant shear will not occur because the O3′ ↔ α-O1 paths in Figure 11 (depicted as solid lines) do not have infinite connectivity. Such a preference could arise from a greater thermodynamic stability of α-O1 over β-O1 or from differences in the kinetics of O3′ → α-O1 and O3′ → β-O1 transformations.

The above analysis of lattice-invariant shear applies equally to the staged "hybrid" structures seen in many intercalation compounds. For example, around $x \approx 0.15$, Li_xCoO_2 forms a staged O1/O3 hybrid (also referred to as H1−3),[37,38] wherein the Li resides in O3-like layers while the O1-like layers are empty. The above analysis indicates that lattice-invariant shear occurs in O3 ↔ O1/O3 transformations and O1 ↔ O1/O3

DOI: 10.1021/acs.nanolett.7b03989
Nano Lett. XXXX, XXX, XXX−XXX

transformations just as it does in O3 ↔ O1 transformations; this is because the gliding of neighboring layers to O1 or O3 stackings does not break the symmetry between equivalent glides of a given layer. Similarly, lattice-invariant shear is expected in transformations involving O1/P3, O3/P3, and O2/P2 hybrids in Na layered oxides and sulfides[17,58] as well as transformations involving hybrid staged phases in Li-intercalated graphite.[12,14,59]

Conclusion. We conclude by discussing the implications of electrochemical creep for the design of batteries and other devices based on layered materials. Because the H1−3 and O1 phases in the layered oxides only occur at very high states of charge, they are typically not accessed in the operation of practical Li-ion batteries, where charging is usually restricted to ∼4.3 V in order to preserve cycle life.[4] In contrast, we expect electrochemical creep to occur in the graphitic anodes of practical Li-ion batteries, where transformations between staged phases occur at compositions that are accessed during normal operation.[12,14,59] Electrochemical creep may be more important, however, for Na-ion battery materials than Li-ion materials because of the greater propensity for stacking-sequence changes in layered Na compounds.[4−6,16,17]

Traditional strategies for preventing degradation associated with stacking-sequence-change phase transformations focus on suppressing phase transformation altogether, either by restricting the state of charge[3,4,23] or introducing dopants that discourage stacking sequence changes.[16] Our analysis suggests, however, that suppressing all phase transitions may be unnecessary: electrochemical creep potentially can be prevented by lowering the symmetry of the crystal, for example, by tuning the composition or synthesis conditions to achieve cation ordering in the transition-metal layer.

■ ASSOCIATED CONTENT

Supporting Information

The Supporting Information is available free of charge on the ACS Publications website at DOI: 10.1021/acs.nanolett.7b03989.

Definition of vector space describing stacking-sequence changes and analysis of roughness generated by lattice-invariant shear in layered materials (PDF)

■ AUTHOR INFORMATION

Corresponding Author

*E-mail: avdv@engineering.ucsb.edu.

ORCID

Maxwell D. Radin: 0000-0002-8989-8114

Y. Shirley Meng: 0000-0001-8936-8845

Notes

The authors declare no competing financial interest.

■ ACKNOWLEDGMENTS

This work was supported as part of the NorthEast Center for Chemical Energy Storage (NECCES), an Energy Frontier Research Center funded by the U.S. Department of Energy, Office of Science, Basic Energy Sciences under Award No. DE-SC0012583.

■ REFERENCES

(1) Pollard, A. M.; Heron, C. *Archaeological chemistry*, 2nd ed.; The Royal Society of Chemistry: Cambridge, U.K., 2008.

(2) Crabtree, G.; Kócs, E.; Trahey, L. *MRS Bull.* **2015**, *40*, 1067−1078.

(3) Whittingham, M. S. *Chem. Rev.* **2004**, *104*, 4271−4302.

(4) Radin, M. D.; Hy, S.; Sina, M.; Fang, C.; Liu, H.; Vinckeviciute, J.; Zhang, M.; Whittingham, M. S.; Meng, Y. S.; Van der Ven, A. *Adv. Energy Mater.* **2017**, *7*, 1602888.

(5) Han, M. H.; Gonzalo, E.; Singh, G.; Rojo, T. *Energy Environ. Sci.* **2015**, *8*, 81−102.

(6) Yabuuchi, N.; Kubota, K.; Dahbi, M.; Komaba, S. *Chem. Rev.* **2014**, *114*, 11636−11682.

(7) Wang, Q. H.; Kalantar-Zadeh, K.; Kis, A.; Coleman, J. N.; Strano, M. S. *Nat. Nanotechnol.* **2012**, *7*, 699−712.

(8) Clauss, F. J. *Solid lubricants and self-lubricating solids*; Academic Press: New York, 1972.

(9) Nalawade, P.; Aware, B.; Kadam, V. J.; Hirlekar, R. S. *Ind. Res.* **2009**, *68*, 267−272.

(10) Amatucci, G. G.; Tarascon, J. M.; Klein, L. C. *J. Electrochem. Soc.* **1996**, *143*, 1114−1123.

(11) Van der Ven, A.; Aydinol, M. K.; Ceder, G.; Kresse, G.; Hafner, J. *Phys. Rev. B: Condens. Matter Mater. Phys.* **1998**, *58*, 2975−2987.

(12) Dahn, J. R. *Phys. Rev. B: Condens. Matter Mater. Phys.* **1991**, *44*, 9170−9177.

(13) Ohzuku, T.; Iwakoshi, Y.; Sawai, K. *J. Electrochem. Soc.* **1993**, *140*, 2490.

(14) Woo, K. C.; Kamitakahara, W. A.; DiVincenzo, D. P.; Robinson, D. S.; Mertwoy, H.; Milliken, J. W.; Fischer, J. E. *Phys. Rev. Lett.* **1983**, *50*, 182−185.

(15) Dresselhaus, M. S.; Dresselhaus, G. *Adv. Phys.* **2002**, *51*, 1−186.

(16) Radin, M. D.; Van der Ven, A. *Chem. Mater.* **2016**, *28*, 7898−7904.

(17) Vinckeviciute, J.; Radin, M. D.; Van der Ven, A. *Chem. Mater.* **2016**, *28*, 8640−8650.

(18) Van der Ven, A.; Morgan, D.; Meng, Y. S.; Ceder, G. *J. Electrochem. Soc.* **2006**, *153*, A210−A215.

(19) Casas-Cabanas, M.; Canales-Vázquez, J.; Rodríguez-Carvajal, J.; Palacín, M. R. *J. Am. Chem. Soc.* **2007**, *129*, 5840−5842.

(20) Wang, Y.; Ou, J. Z.; Balendhran, S.; Chrimes, A. F.; Mortazavi, M.; Yao, D. D.; Field, M. R.; Latham, K.; Bansal, V.; Friend, J. R.; Zhuiykov, S.; Medhekar, N. V.; Strano, M. S.; Kalantar-Zadeh, K. *ACS Nano* **2013**, *7*, 10083−10093.

(21) Xiong, F.; Wang, H.; Liu, X.; Sun, J.; Brongersma, M.; Pop, E.; Cui, Y. *Nano Lett.* **2015**, *15*, 6777−6784.

(22) Duerloo, K.-A. N.; Li, Y.; Reed, E. J. *Nat. Commun.* **2014**, *5*, 4214.

(23) Yin, S. C.; Rho, Y. H.; Swainson, I.; Nazar, L. F. *Chem. Mater.* **2006**, *18*, 1901−1910.

(24) Yazami, R.; Ozawa, Y.; Gabrisch, H.; Fultz, B. *Electrochim. Acta* **2004**, *50*, 385−390.

(25) Wang, H.; Jang, Y.; Huang, B.; Sadoway, D. R.; Chiang, Y. *J. Electrochem. Soc.* **1999**, *146*, 473−480.

(26) Woodford, W. H.; Carter, W. C.; Chiang, Y.-M. *Energy Environ. Sci.* **2012**, *5*, 8014.

(27) Liu, H.; Wolf, M.; Karki, K.; Yu, Y. S.; Stach, E. A.; Cabana, J.; Chapman, K. W.; Chupas, P. J. *Nano Lett.* **2017**, *17*, 3452−3457.

(28) Yano, A.; Shikano, M.; Ueda, A.; Sakaebe, H.; Ogumi, Z. *J. Electrochem. Soc.* **2017**, *164*, A6116−A6122.

(29) Mukhopadhyay, A.; Sheldon, B. W. *Prog. Mater. Sci.* **2014**, *63*, 58−116.

(30) Woodford, W. H.; Chiang, Y.-M.; Carter, W. C. *J. Electrochem. Soc.* **2010**, *157*, A1052−A1059.

(31) Bhattacharya, K.; Conti, S.; Zanzotto, G.; Zimmer, J. *Nature* **2004**, *428*, 55−59.

(32) Porter, D. A.; Easterling, K. E.; Sherif, M. Y. *Phase transformations in metals and alloys*; CRC Press: Boca Raton, FL, 2009.

(33) Bhattacharya, K. *Microstructure of martensite : why it forms and how it gives rise to the shape-memory effect*; Oxford University Press: Oxford, 2003.

(34) Otsuka, K.; Ren, X. *Prog. Mater. Sci.* **2005**, *50*, 511−678.

DOI: 10.1021/acs.nanolett.7b03989
Nano Lett. XXXX, XXX, XXX−XXX

(35) Andre, D.; Kim, S.-J.; Lamp, P.; Lux, S. F.; Maglia, F.; Paschos, O.; Stiaszny, B. *J. Mater. Chem. A* **2015**, *3*, 6709−6732.
(36) Nitta, N.; Wu, F.; Lee, J. T.; Yushin, G. *Mater. Today* **2015**, *18*, 252−264.
(37) Van der Ven, A.; Aydinol, M. K.; Ceder, G. *J. Electrochem. Soc.* **1998**, *145*, 2149−2155.
(38) Chen, Z.; Lu, Z.; Dahn, J. R. *J. Electrochem. Soc.* **2002**, *149*, A1604−A1609.
(39) Delmas, C.; Fouassier, C.; Hagenmuller, P. *Physica B+C* **1980**, *99*, 81−85.
(40) Tournadre, F.; Croguennec, L.; Saadoune, I.; Carlier, D.; Shao-Horn, Y.; Willmann, P.; Delmas, C. *J. Solid State Chem.* **2004**, *177*, 2790−2802.
(41) Croguennec, L.; Pouillerie, C.; Mansour, a. N.; Delmas, C. *J. Mater. Chem.* **2001**, *11*, 131−141.
(42) Lee, D. H.; Xu, J.; Meng, Y. S. *Phys. Chem. Chem. Phys.* **2013**, *15*, 3304−3312.
(43) Gabrisch, H.; Yazami, R.; Fultz, B. *Electrochem. Solid-State Lett.* **2002**, *5*, A111.
(44) Krupp, U. *Fatigue crack propagation in metals and alloys : microstructural aspects and modelling concepts*; Wiley-VCH: Weinheim, 2007.
(45) Sangid, M. D. *Int. J. Fatigue* **2013**, *57*, 58−72.
(46) Lu, Z.; Dahn, J. R. *J. Electrochem. Soc.* **2001**, *148*, A1225.
(47) Lee, D. H.; Xu, J.; Meng, Y. S. *Phys. Chem. Chem. Phys.* **2013**, *15*, 3304.
(48) Alvarado, J.; Ma, C.; Wang, S.; Nguyen, K.; Kodur, M.; Meng, Y. S. *ACS Appl. Mater. Interfaces* **2017**, *9*, 26518−26530.
(49) Yabuuchi, N.; Kawamoto, Y.; Hara, R.; Ishigaki, T.; Hoshikawa, A.; Yonemura, M.; Kamiyama, T.; Komaba, S. *Inorg. Chem.* **2013**, *52*, 9131−9142.
(50) Marianetti, C.; Morgan, D.; Ceder, G. *Phys. Rev. B: Condens. Matter Mater. Phys.* **2001**, *63*, 1−15.
(51) Reimers, J. N.; Dahn, J. R. *J. Electrochem. Soc.* **1992**, *139*, 2091−2097.
(52) Toumar, A. J.; Ong, S. P.; Richards, W. D.; Dacek, S.; Ceder, G. *Phys. Rev. Appl.* **2015**, *4*, 64002.
(53) Hy, S.; Liu, H.; Qian, D.; Zhang, M.; Hwang, B. J.; Meng, Y. S. *Energy Environ. Sci.* **2016**, *9*, 1931−1954.
(54) Hong, J.; Gwon, H.; Jung, S.-K.; Ku, K.; Kang, K. *J. Electrochem. Soc.* **2015**, *162*, A2447−A2467.
(55) Rozier, P.; Tarascon, J. M. *J. Electrochem. Soc.* **2015**, *162*, A2490−A2499.
(56) Kim, J.-S.; Johnson, C. S.; Vaughey, J. T.; Thackeray, M. M.; Hackney, S. A.; Yoon, W.; Grey, C. P. *Chem. Mater.* **2004**, *16*, 1996−2006.
(57) Lu, Z.; Beaulieu, L. Y.; Donaberger, R. A.; Thomas, C. L.; Dahn, J. R. *J. Electrochem. Soc.* **2002**, *149*, A778.
(58) Yabuuchi, N.; Kajiyama, M.; Iwatate, J.; Nishikawa, H.; Hitomi, S.; Okuyama, R.; Usui, R.; Yamada, Y.; Komaba, S. *Nat. Mater.* **2012**, *11*, 512−517.
(59) Guerard, D.; Herold, A. *Carbon* **1975**, *13*, 337−345.

DOI: 10.1021/acs.nanolett.7b03989
Nano Lett. XXXX, XXX, XXX−XXX